Available online at www.sciencedirect.com
SCIENCE DIRECT®
C. R. Mecanique 332 (2004) 413–428
COMPTES RENDUS MECANIQUE

Microgravity and transfers/Solidification, crystal growth from the melt

Recent developments in Liquid Phase Electroepitaxial growth of bulk crystals under magnetic field

Sadik Dost [a,*], Brian Lent [b], Hamdi Sheibani [a,b], Yongcai Liu [a]

[a] *Crystal Growth Laboratory, University of Victoria, Victoria V8W 3P6, BC, Canada*
[b] *DL Crystals Inc., R-Hut, McKenzie Road, Victoria V8W 3W2, BC, Canada*

Available online 10 April 2004

Abstract

This review article presents recent developments in Liquid Phase Electroepitaxial (LPEE) growth of bulk single crystals of alloy semiconductors under an applied static magnetic field. The growth rate in LPEE is proportional to the applied electric current. However, at higher electric current levels the growth becomes unstable due to the strong convection occurring in the liquid zone. In order to address this problem, a significant body of research has been performed in recent years to suppress and control the natural convection for the purpose of prolonging the growth process to grow larger crystals. LPEE growth experiments show that the growth rate under an applied static magnetic field is also proportional and increases with the field intensity level. The modeling of LPEE growth under magnetic field was also the subject of interest. Two-dimensional mathematical models developed for the LPEE growth process predicted that the natural convection in the liquid zone would be suppressed almost completely with increasing the magnetic field level. However, experiments and also three-dimensional models have shown that there is an optimum magnetic field level below which the growth process is stable and the convection in the liquid zone is suppressed, but above such a field level the convective flow becomes very strong and leads to unstable growth with unstable interfaces. ***To cite this article: S. Dost et al., C. R. Mecanique 332 (2004).***

Résumé

Développements récents en cristallogénèse par Electro-Epitaxie en Phase Liquide (LPEE) sous l'effet d'un champ magnétique. Cet article présente une revue des développements récents en cristallogénèse par Electro-Epitaxie en Phase Liquide (LPEE), des monocristaux d'alliages semi-conducteurs, sous l'effet d'un champ magnétique statique. La vitesse de croissance est proportionnelle à l'intensité du courant électrique. Néanmoins, pour des courants élevés, la croissance devient instable, à cause de la convection forte dans la zone liquide. Il y a eu beaucoup de recherches ces dernières années pour diminuer et maîtriser la convection naturelle et faire croître des cristaux plus grands. Les expériences de croissance par LPEE montrent que la vitesse de croissance sous champ magnétique est proportionnelle, à l'intensité du champ magnétique. La simulation numérique de la croissance par LPEE en présence d'un champ magnétique, fut également, un important objet de recherche. Les simulations numériques, en deux dimensions, prévoient que la convection naturelle est quasiment supprimée lorsque l'intensité du champ magnétique s'accroît fortement. Or, des expériences et simulations tri-dimensionnelles montrent l'existence d'une valeur de l'intensité magnétique au-dessous de laquelle la croissance est stable et la convection est supprimée ; mais, à des

* Corresponding author.
E-mail address: sdost@me.uvic.ca (S. Dost).

1631-0721/$ – see front matter
doi:10.1016/j.crme.2004.02.019

intensités plus élevées, l'influence de la convection est très forte, ce qui conduit à une croissance irrégulière et des interfaces instables. ***Pour citer cet article : S. Dost et al., C. R. Mecanique 332 (2004).***

Keywords: Instability; Magnetic field; Convection; Crystal growth; Electroepitaxy

Mots-clés : Instabilité ; Champ magnétique ; Convection ; Cristallogénèse ; Électro-épitaxie

1. Introduction

Liquid Phase Electroepitaxy (LPEE), being a solution growth, has a number of advantages over other bulk crystal growth techniques. For instance, the growth furnace temperatures used are relatively lower, the temperature gradient in the LPEE solution zone is very small, less than a few °C/cm, LPEE has the ability of well-controlled growth, by simply controlling the applied electric current, and ternary single crystals can be grown with uniform compositions. Such features of LPEE make this technique technologically very promising (see, for instance, [1–9]), and it has a great potential to become a commercial technique in growing high quality, bulk crystals such as GaInAs, GaInSb, CdZnTe, SiGe (see [10–13]).

However, in spite of such significant advantages, LPEE has thus far suffered from mainly three 'shortfalls' toward its commercialization. The first is the achievable crystal thickness that is relatively small, in the order of a few millimeters [1–12]. This is mainly due to the combined effect of Peltier and Joule heating in the system, leading to temperature gradients and a relatively strong natural convection in the liquid solution zone that causes unsatisfactory and unstable growth. This puts a limit on the achievable crystal thickness, particularly in the growth of *bulk* crystals, and provides less useful material for use. The second shortfall of LPEE has been its low growth rate. The growth rate in LPEE is almost linearly proportional with the applied electric current, and is about 0.5 mm/day at a 3 A/cm^2 electric current density [14,15]. Of course, for higher electric current density levels, the growth rate increases, but in growth of thick (bulk) crystals the combined effect of temperature gradients and natural convection leads to unstable growth, and the growth stops. This was the main reason why many researchers have given up on LPEE, losing their hope for its development towards commercialization to compete with other bulk techniques. The third shortfall of LPEE is the need for a single crystal seed of the same composition of the crystal to be grown. Small compositional differences, in the order of 4% depending on the crystal lattice parameters, can be tolerated, but higher compositional differences may lead to unsatisfactory growth.

The experimental work conducted in [14,15] on the LPEE growth of ternary InGaAs single crystals has addressed the first two 'shortfalls' of LPEE. By optimizing the growth parameters of LPEE, and also by using a static external applied magnetic field, a number of bulk (thick), flat GaAs single crystals and $In_{0.04}Ga_{0.96}As$ single crystals of uniform compositions were grown, and the growth rate of LPEE was increased more than 10 times for a selected electric current density. The grown crystals were all single crystals, and the results were reproducible in terms of crystal thickness, growth rate, and compositional uniformity. The third 'shortfall' of LPEE will be addressed in future research, using some other means such as a 'bootstrapping' process with small incremental changes in composition, a new technique such as liquid phase diffusion, etc.

In LPEE, growth is achieved by passing an electric current through the growth cell while the overall furnace temperature is kept constant during the entire growth period (see Fig. 1). The applied electric current is the sole driving force for growth, and gives rise to two growth mechanisms that are known as 'electromigration' and 'Peltier cooling/heating'. Although the electromigration of species (components) in the liquid solution in LPEE was attributed to electron-momentum exchange and electrostatic field forces [1,2], there is still no rational model in the literature explaining this mechanism. However, whatever the reason behind this mechanism, the electromigration of species sustains a controlled-growth in LPEE [14,15]. The Peltier heating/cooling, on the other hand, is a thermoelectric effect occurring when an electric current passes through an interface between two materials with different Peltier coefficients. The Peltier cooling at the growth interface undercools the solution in the immediate

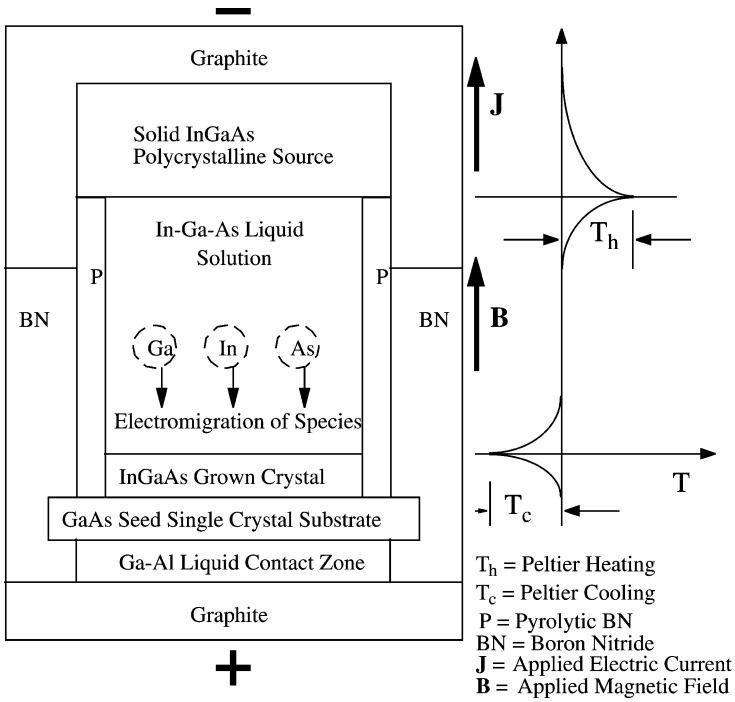

Fig. 1. Schematic view of the experimental LPEE growth crucible. The electric and magnetic fields are also shown in the figure. Although in the model a Ga–As solution is considered for simplicity, the LPEE system of GaInAs was given in this figure for completeness.

vicinity of the substrate and leads to epitaxial growth. The Peltier heating at the dissolution interface, on the other hand, causes the dissolution of the source material into the solution and constantly provides the needed feed material for growth. The growth rate is proportional to the applied electric current density [1–15].

In a typical LPEE system, although the furnace temperature is constant as mentioned earlier, the combined effect of the Joule heating in the solid crystals and the Peltier heating/cooling at the growth and dissolution interfaces leads to relatively small temperature gradients in the solution. Such temperature gradients, together with concentration gradients, result in a significant natural convection in the solution. This convective flow in the solution has an adverse effect on the LPEE growth process [16]. It leads to interface instability and consequently stops the growth. This limits the crystals thickness and growth rate.

In order to suppress the adverse effect of convection, the LPEE growth of single crystals under a static applied magnetic field has been studied both numerically and experimentally. The related modeling and numerical studies can be found in [8,13,16–24], and the details of the experimental results can be found in [14,15]. The objective of the earlier modeling studies was to examine the effect of an applied static magnetic field in minimizing the adverse effect of the natural convection in the liquid solution. These studies have shown that lower convection in the solution may allow the use of higher electric current densities that will be translated into higher growth rates. A detailed account of application of magnetic field and related literature can be found in [25–27].

The numerical simulations performed in [8,13,16–24,28,30] were two-dimensional, and resulted in a conclusion that the convection in the liquid zone can be suppressed completely by simply increasing the magnetic field intensity level. Considering the complexity of the LPEE growth system, such a result did not seem to be physically admissible. In fact, the three-dimensional numerical simulation results in [27] have shown that this is not the case at all, and there are three distinct levels of magnetic field intensities that are affecting the flow structures differently. Field intensities up to 2.0 kGauss suppress the flow structures in the solution, and the flow structures are stable and get weaker with the increasing magnetic field level. These levels of magnetic field are beneficial in suppressing the

natural convection. However, field intensities higher than 2.0 kGauss change the flow patterns significantly, and at intensities higher than 3.0 kGauss the flow structures become unstable [27].

In fact the experimental study of the LPEE growth of GaAs and $Ga_{0.96}In_{0.04}As$ single crystals [14,15] supported qualitatively the results of these three-dimensional numerical simulations. Experimental results of [14,15] can be summarized as follows. Their newly developed LPEE growth system allowed the growth of a large number of GaAs and $Ga_{0.96}In_{0.04}As$ single crystals of thicknesses up to 9 mm. It was possible to apply electric current densities of 3, 5, and 7 A/cm^2, and the corresponding growth rates in these experiments with no magnetic field were respectively about 0.57, 0.75 and 1.25 mm/day. Growth interfaces were very flat, and the growth experiments were reproducible in terms of crystal thickness and growth rate. Experiments at higher electric current intensities were not successful.

Experiments at 3, 5 and 7 A/cm^2 electric current densities were repeated under various applied static magnetic field levels [15]. Results showed that LPEE experiments at the 4.5 kGauss and lower magnetic field levels are successful, but those under higher magnetic field levels were not [15,24]. It seems that the 4.5 kGauss field level is a maximum ('critical') above which the growth is not stable. This experimental 'critical' magnetic field level is higher than that predicted from the numerical simulations performed under the same growth conditions, which was about 2.0–3.0 kGauss [27]. Considering the complexity of the LPEE growth process, this is a good qualitative agreement.

As mentioned above, the LPEE experiments presented in [14,15] have shed light on the issue of the presence of an optimum applied magnetic field in suppressing convection for prolonging the LPEE growth for larger crystals, and supported the observations from three-dimensional simulation models. However, the LPEE experiments in [15] yielded a very significant result that was not predicted (or expected) from the modeling studies conducted so far: the experimental LPEE growth rates under magnetic field were much higher than the expected values. For instance, the growth rate at 4.5 kGauss magnetic field level (at $J = 3$ A/cm^2) was about 6.1 mm/day, which is about 12 times higher than that with no magnetic field. Experiments performed at $B = 1.0$ and 2.0 kGauss field levels (at $J = 3$ A/cm^2) were also successful, and the growth rates were also higher: 1.62 and 2.35 mm/day, respectively. Such growth rates have not been predicted from any models so far. One more interesting observation of the LPEE experiments was that the direction of the applied magnetic field, either up or down, was not relevant. The growth rate was almost the same, being about 5–6% less when the magnetic field was in the direction of the applied electric field [31].

As predicted from the three-dimensional models, at higher magnetic field levels (even with the $J = 3$ A/cm^2 electric current density level), and higher electric current density levels ($J = 10$ A/cm^2 or higher), experiments did not lead to successful growth, but showed very interesting outcomes [24,31]. Although very thick crystals were grown, even up to a 9 mm thickness, the growth processes were not stable and lead to uneven growth. From the visual inspection of the grown crystals, the adverse effect of natural convection was obvious causing either one-sided growth or leading to holes in the grown crystals. It was considered that such a growth (one-sided and with holes) is because of the strong and unstable convection in the liquid zones (solution and contact zones) due to the strong interaction between the applied magnetic field and the applied electric current. Such predictions were also confirmed qualitatively by the numerical simulations carried out by considering field non-uniformities in [27], and also by using a newly defined electromagnetic mobility in [31]. The simulated flow structures show the possibility of causing such non-uniform growth of crystals.

The objective of this article is to review the recent significant developments in LPEE growth of single crystals under magnetic field. Results of experimental and modeling studies conducted to date are summarized, and the theoretical models developed earlier in [7,16,28] are revisited in order to shed light on the issue of high growth rates observed in LPEE. The article also includes recent results of numerical simulations for the LPEE growth of GaAs single crystals.

2. Basic equations

The development of the theoretical models of LPEE growth of binary and ternary systems with and without the inclusion of an applied static magnetic field was presented in [8,16,28]. Details of the development of the basic equations and the associated inherent model assumptions can be found in these articles. The basic equations of the LPEE growth process of a binary system are briefly presented below for the sake of completeness.

Since the LPEE growth process involves the passage of an electric current and also the application of a static magnetic field, the well-known Maxwell equations must also be considered along with the fundamental equations of the thermomechanics. However as can be seen from [8,16,28], since the applied magnetic field is static and assumed to be uniform in the metallic liquid solution (indeed it is almost uniform in the system of [15], less than 1%), and also both the applied magnetic field and the applied electric current are vertical and aligned perfectly with the symmetry axis of the growth system, the Maxwell equations reduce to a single equation [8,16], namely the conservation of charge equation $\nabla \cdot \mathbf{J} = \mathbf{0}$, which leads to a uniform electric field distribution in the liquid phase due to the assumed boundary conditions. However, in a system where these conditions are not satisfied, the Maxwell equations must be solved simultaneously along with the thermomechanical equations. In the system considered here, $\mathbf{J}$ is the total electric current density (in a fixed Galilean frame)

$$\mathbf{J} = \sigma_E \boldsymbol{E} = \sigma_E(\mathbf{E} + \mathbf{v} \times \mathbf{B}) \quad \text{where } \boldsymbol{E} = \mathbf{E} + \mathbf{v} \times \mathbf{B} \tag{1}$$

where the $\boldsymbol{E}$ is the electric field referred to the co-moving frame [16], $\mathbf{E}$, and $\mathbf{B}$ are the electric field and the magnetic induction in a fixed Galilean frame.

In the numerical simulations given in [22,27] small variations in the magnetic and electric fields and also small deviations from the axisymmetry in the LPEE growth system were considered. Numerical results, however, showed that the effects of such variations on transport structures and the growth process were not significant. Therefore, in a well-designed LPEE set up, the above assumption of uniform fields in the solution is justified.

In the models of the literature developed for either binary (such Ga–As) or ternary (such as InGaAs) systems, the liquid phase was assumed to be a non-polarizable, non-magnetizable, Newtonian viscous fluid mixture [16,28], and the magnetohydrodynamic approximation holds (see [29] for details). The thermomechanical balance laws of a binary medium, namely the overall conservation of mass, the balance of linear momentum, the conservation of mass for the solute (which is As in a Ga-rich solvent), the balance of energy, and the second laws of thermodynamics yield the general local balance equations which can be found in [16,28].

In this section we present the model equations for the growth of GaAs crystals by LPEE under an applied magnetic field. A schematic view of the LPEE growth crucible is shown in Fig. 1. The field equations of the liquid phase are obtained as

Continuity

$$\nabla \cdot \mathbf{v} = 0 \tag{2}$$

Momentum

$$-\nabla p + 2\mu_v \nabla \cdot \mathbf{d} + \mathbf{g}\{-\rho_L \beta_T (T - T_0) + \rho_L \beta_C (C - C_0)\} + \sigma_E \boldsymbol{E} \times \mathbf{B} = \rho_L \left(\frac{\partial \mathbf{v}}{\partial t} + \mathbf{v} \cdot \nabla \mathbf{v} \right) \tag{3}$$

Mass Transport

$$(\mu_E + \mu_E)\boldsymbol{E} \cdot \nabla C + D_C \nabla^2 C = \frac{\partial C}{\partial t} + \mathbf{v} \cdot \nabla C \tag{4}$$

Energy

$$k_T \nabla^2 T = \rho_L \gamma_L \left(\frac{\partial T}{\partial t} + \mathbf{v} \cdot \nabla T \right) \tag{5}$$

where ρ_L denotes the constant density of the binary mixture defined in terms of densities of the solute ρ_1 and the solvent ρ_2 by $\rho_L = \rho_1 + \rho_2$, C, is the mass concentration of the solute defined by $C = \rho_1/\rho$, p is the pressure,

and T denotes temperature. The vector $\sigma_E \boldsymbol{E} \times \mathbf{B}$ represents the magnetic body force [29] which was obtained from $\mathbf{J} \times \mathbf{B}$ under the assumption of negligible convection current. σ_E and k_T are the electric and thermal conductivities, respectively. μ_v is the viscosity, and γ_L represents the specific heat of the liquid solution. $\mathbf{d}$ is the deformation rate tensor given by $2\mathbf{d} = \nabla\mathbf{v} + (\nabla\mathbf{v})^{\mathrm{T}}$ where T denotes transpose, ∇ is the nabla operator, and $\mathbf{v}$ stands for the velocity vector. In the derivation of Eqs. (2)–(5), the following assumptions and simplifications were made.

(i) It was assumed that the so-called Boussinesq approximation holds. That is, in order to allow density variations we assume that the density of the liquid phase is constant everywhere in the field equations except in the gravitational body force, i.e.,

$$\rho\mathbf{f} = -\mathbf{g}\big\{\rho_L\beta_T(T - T_0) + \rho_L\beta_C(C - C_0)\big\} \tag{6}$$

where β_T and β_C are the thermal and solutal expansion coefficients, respectively, and T_0 and C_0 are the reference temperature and concentration.

(ii) In the LPEE crucible used in [15], as mentioned earlier, the electric field and the magnetic field are aligned vertically and considered uniform. This satisfies the only remaining Maxwell equation, i.e., $\nabla \cdot \mathbf{J} = \mathbf{0}$ identically. Otherwise, the electric field in the solution will be obtained from the solution of $\nabla \cdot \mathbf{J} = \mathbf{0}$, as was the case in [22, 27]. Since the electric field was almost uniform in [22,27], the electric current distribution is considered uniform for computational convenience. In addition the induced magnetic field due to the applied electric current is small, so is neglected.

(iii) In the constitutive equations, we assumed further simplifications to those of [16], namely (a) some of the second order material constants are small; (b) the contributions of the well-known Soret and Dufour effects are negligible; (c) the contribution of temperature and concentration variations to the electric current is small; but (d) the second and third order contributions of the electric current and magnetic field intensity to the mass flux are not negligible. Under these assumptions, the following mass flux was used

$$\mathbf{i} = \rho_0(\mu_{EC} + \mu_{ECB})C\boldsymbol{E} + \rho_0 D_C \nabla C \tag{7}$$

where B is the magnetic field intensity, and

$$\mu_{EC} \equiv \mu_E \quad \text{and} \quad \mu_{ECB} \equiv \mu_B = \bar{\mu}_B B \tag{8}$$

are the second and third order material coefficients representing, respectively, the contributions of the applied electric current and the applied magnetic field.

In Fig. 1 the applied static magnetic field is shown upwards, but the LPEE growth experiments show that [14,15] the growth is in the direction of the applied electric current, and the growth rate is almost the same regardless whether the applied magnetic field is upward or downward. This eliminates the possibility of the explicit dependence of the mass flux in Eq. (7) on the magnetic field vector. As mentioned earlier, in the linearization, all the materials constants in the constitutive equations were assumed to be functions of the reference temperature and concentrations only. In [31], it was shown that the mass flux must depends on the magnetic field in the form given in Eqs. (7) and (8). The material constant μ_E is the well-known *electric mobility*. The new B-dependent coefficient μ_B is called the *magnetic mobility* [31], and has a significant contribution to the mass transport in LPEE. This is similarly to the nonlinear effects considered in [32,33] for the contribution of temperature gradient to mass transport (for the inclusion of the Soret effect). Here, such effects were not considered since the LPEE growth process is almost isothermal (the applied electric current is the only driving force for growth; there is no growth in the absence of the applied electric current and the contribution of the temperature gradient is insignificant). The contribution of diffusion is very small compared with that of the electromigration.

(iv) The heat source in the liquid zone is neglected since the liquid is a good conductor. In addition, the contributions of the electric field and concentration gradient to the heat flux are also assumed small.

(v) Finally, the metallic solution is assumed to be a non-polarizable, non-magnetizable, incompressible, and Newtonian viscous liquid.

The first term in Eq. (4) represents the contribution of the applied electric current density to mass transport. This is known as *electromigration*. The material constant, μ_E, is the mobility of the solute (As) in the liquid solution

Table 1
Mobility values

Magnetic field B (kGauss)	0.0	1.0	2.0	4.5
Electric current (A/cm^2)	3.0	3.0	3.0	3.0
Growth rate (mm/day)	0.5	1.62	2.35	6.1
Total mobility $\mu_{\text{total}} = \mu_E + \mu_B$ (m^2/Vs)	0.68×10^{-5}	2.30×10^{-5}	3.40×10^{-5}	7.10×10^{-5}
Constant electric mobility μ_E (m^2/Vs)	0.68×10^{-5}	0.68×10^{-5}	0.68×10^{-5}	0.68×10^{-5}
Electromagnetic mobility $\mu_B = \bar{\mu}_B B$ (m^2/Vs)	0.0	1.62×10^{-5}	2.72×10^{-5}	6.42×10^{-5}

(Ga–As solution) due to the applied electric current. Experiments show that the growth rate in LPEE is proportional with the applied electric current density and the value of μ_E in the Ga–As (and also in In–Ga–As) solution was evaluated in [15,23,24]. The numerical value of μ_E is given in Table 1. As will be seen later, the numerical simulations based on this value verify the experimental growth rates at all three electric current levels ($J = 3, 5$, and 7 A/cm^2) in the absence of an applied magnetic field. In other words, μ_E is a known material constant in LPEE growth of GaAs. Of course, the diffusion (third term, $D_C \nabla^2 C$) and also the natural convection (the last term on the right-hand side, $\mathbf{v} \cdot \nabla C$) contribute to the growth rate [8,16–24]. However, in LPEE the contribution of the first term (electromigration) is dominant [8], and the growth rate is almost proportional with this term.

In the present model, the influence of the applied magnetic field is incorporated into Eq. (4) through the term $\mu_B \boldsymbol{E} \cdot \nabla C$. Since the applied static magnetic field and the electric current are aligned with the vertical axis of the growth system, i.e., $\mathbf{B} = B\mathbf{e_z}$, $\mathbf{E} = E_z \mathbf{e_z} = (J/\sigma_E)\mathbf{e_z}$, Eqs. (1) and (7) yield

$$\mathbf{J} = \sigma\left(Bv\mathbf{e_r} - Bu\mathbf{e}_\varphi + \frac{J}{\sigma}\mathbf{e_z}\right) \quad \text{and} \quad \sigma_E \boldsymbol{E} \times \mathbf{B} = \sigma_E(\mathbf{v} \times \mathbf{B}) \times \mathbf{B} - \sigma_E B^2(u\mathbf{e_r} + v\mathbf{e}_\varphi) \tag{9}$$

The first term in Eq. (4) is now written as

$$(\mu_E + \mu_B)(\mathbf{E} + \mathbf{v} \times \mathbf{B}) \cdot \nabla C \tag{10}$$

Since the term $(\mathbf{v} \times \mathbf{B}) \cdot \nabla C$ is small compared with $\mathbf{E} \cdot \nabla C$ (in the order of 3% based on a maximum velocity of 0.01 m/s and a 10 kGauss field level), it is neglected for simplicity. Then we write

$$(\mu_E + \mu_B) E_z \frac{\partial C}{\partial z} = \mu_{\text{total}} E_z \frac{\partial C}{\partial z} \tag{11}$$

The numerical values of the total mobility $\mu_{\text{total}} = \mu_E + \mu_B$ are given in Table 1 for different magnetic field levels. As mentioned earlier, although is a material constant that is not dependent on the applied electric current, the electromagnetic mobility μ_B, by definition, depends on the magnetic field intensity (appears to be linearly), but not on its direction. The values of μ_B are almost the same whether $\mathbf{B}$ is up or down. The difference in experimental values of μ_B when $\mathbf{B}$ is in the opposite direction to $\mathbf{E}$ is very small, about 5–6% based on the measured crystal thicknesses. It is possible that this difference is partly due to measurement errors and partly due to the contribution of the term $(\mathbf{v} \times \mathbf{B}) \cdot \nabla C$ that was neglected in the numerical simulation model. But for all practical purposes in the model, it is assumed that the growth rate is the same in both cases. It should also be noted that in the LPEE system considered here [15] the magnetic body force components in Eq. (9) are not dependent on the direction of $\mathbf{B}$.

The growth rate at the growth interface is calculated by [22]

$$V_g = \frac{\rho_L}{\rho_S}\left(D_C \frac{\partial C}{\partial n} + \mu_{\text{total}} E_z C\right) \frac{1}{C_S - C} \tag{12}$$

For the LPEE crucible shown in Fig. 1, the field equations of the liquid phase, Eqs. (2)–(5), take the following explicit forms in the cylindrical coordinate system:

Continuity

$$\frac{1}{r}\frac{\partial}{\partial r}(ru) + \frac{1}{r}\frac{\partial v}{\partial \varphi} + \frac{\partial w}{\partial z} = 0 \tag{13}$$

Momentum

$$\frac{\partial u}{\partial t}+u\frac{\partial u}{\partial r}+\frac{v}{r}\frac{\partial u}{\partial \varphi}+w\frac{\partial u}{\partial z}-\frac{v^2}{r}=\nu\left(\nabla^2 u-\frac{u}{r^2}-\frac{2}{r^2}\frac{\partial v}{\partial \varphi}\right)-\frac{1}{\rho_L}\frac{\partial p}{\partial r}-\frac{\sigma_E}{\rho_L}B^2u \tag{14}$$

$$\frac{\partial v}{\partial t}+u\frac{\partial v}{\partial r}+\frac{v}{r}\frac{\partial v}{\partial \varphi}+w\frac{\partial v}{\partial z}+\frac{uv}{r}=\nu\left(\nabla^2 v-\frac{v}{r^2}+\frac{2}{r^2}\frac{\partial v}{\partial \varphi}\right)-\frac{1}{\rho_L r}\frac{\partial p}{\partial \varphi}-\frac{\sigma_E}{\rho_L}B^2v \tag{15}$$

$$\frac{\partial w}{\partial t}+u\frac{\partial w}{\partial r}+\frac{v}{r}\frac{\partial w}{\partial \varphi}+w\frac{\partial w}{\partial z}=\nu\nabla^2 w-\frac{1}{\rho_L}\frac{\partial p}{\partial z}-g\beta_T(T-T_0)-g\beta_C(C-C_0) \tag{16}$$

Mass transport

$$\frac{\partial C}{\partial t}+u\frac{\partial C}{\partial r}+\frac{v}{r}\frac{\partial C}{\partial \varphi}+w\frac{\partial C}{\partial z}+\mu_{\text{total}}E_z\frac{\partial C}{\partial z}=D_C\nabla^2 C \tag{17}$$

Energy

$$\frac{\partial T}{\partial t}+u\frac{\partial T}{\partial r}+\frac{v}{r}\frac{\partial T}{\partial \varphi}+w\frac{\partial T}{\partial z}=\alpha\nabla^2 T \tag{18}$$

with the ∇^2 operator defined by

$$\nabla^2=\frac{1}{r}\frac{\partial}{\partial r}\left(r\frac{\partial}{\partial r}\right)+\frac{1}{r^2}\frac{\partial^2}{\partial \varphi^2}+\frac{\partial^2}{\partial z^2} \tag{19}$$

where u, v and w are respectively the velocity components in the radial (r), circumferential (φ) and vertical (z) directions. ν is the kinematic viscosity, p is the pressure, and α is the thermal diffusivity.

The axisymmetric boundary and interface conditions take the following forms:

Along the vertical wall

$$u=0,\quad v=0,\quad w=0,\quad T=T_g-\left(\frac{z}{H}\right)\Delta T,\quad \frac{\partial C}{\partial r}=0 \tag{20}$$

Along the growth interface

$$u=0,\quad v=0,\quad w=0,\quad k_s\frac{\partial T}{\partial z}-k_l\frac{\partial T}{\partial z}=-\pi_p J,\quad C=C_1 \tag{21}$$

Along the dissolution interface

$$u=0,\quad v=0,\quad w=0,\quad k_l\frac{\partial T}{\partial z}-k_s\frac{\partial T}{\partial z}=+\pi_p J,\quad C=C_2 \tag{22}$$

In the above equations π_p is the Peltier coefficient, J is the applied electric current density, H is the height of the solution zone along the vertical axis, k_s and k_l are respectively the thermal conductivities of the solid and liquid phases. C_1 and C_2 are respectively the solute concentrations at the growth and dissolution interfaces, which are determined by the interfacial equilibrium conditions (from the phase diagram, see [22,27]). ΔT is the difference between the dissolution and growth interface temperatures relative to the growth temperature T_g (the constant furnace temperature). This is mainly due to the combined effect of the Joule heating and Peltier heating/cooling in the system. Its value is estimated by considering the heat transfer through the whole LPEE system [22,27]. It was assumed that the contribution of latent heat is negligible since the growth rate is very low [28].

The *initial conditions* are

$$C=C_0,\quad u=0,\quad v=0,\quad w=0,\quad \text{and}\quad T=T_g\quad \text{at } t=0 \tag{23}$$

3. Numerical technique

The commercial CFX software is used to solve the three-dimensional governing equations of the model. The computation mesh in the liquid is $120 \times 40 \times 80$ in the r-, φ-, and z-directions, respectively, which is demonstrated to be sufficient for an accurate and stable solution. The evolution of the growth and dissolution interfaces was included in the computations. Several user-defined Fortran subroutines were developed and used in dealing with the moving grid with time, and also with the additional terms related to the electric field in the mass transport equation, and complex thermal boundary conditions. All the field equations were solved simultaneously. It was proven reliable in [27] to carry out simulations for the half cylindrical domain for computational efficiency.

4. Results and discussion

The physical and geometrical data used here are summarized in Table 2. The field equations given in Eqs. (13)–(17) were solved numerically under various electric current density and magnetic field levels, considering only the contribution of electric mobility μ_E [22,24]. In [22,24] the evolution of the growth and dissolution interfaces were not taken into account, the interfaces were considered as stationary. The flow field and concentration distribution at $J = 3, 5$ and $7\ \mathrm{A/cm^2}$ but no magnetic field were computed in [27] by taking the evolution of the interfaces into account. Results showed that both the flow patterns and flow intensities are almost the same; there are no significant differences. The conclusion was that the consideration of the interface evolutions did not make a significant difference on the flow patterns and intensities. The maximum temperature in the solution however increased with the electric current density level, about a 1 °C increase from $J = 3$ to $J = 7\ \mathrm{A/cm^2}$. Computed results in [27] have shown clearly the development of 3-D structures in the flow field and concentration distributions.

Computations repeated under various magnetic field intensity and electric current density levels lead to the behaviour of the maximum flow intensity, $U_{\max} = \sqrt{(u^2 + v^2 + w^2)}$ shown in Fig. 2 versus various magnetic field intensity levels (in both kGauss and the Hartmann number $Ha = BH\sqrt{\sigma_E/\rho_L \nu}$) [24,27,31]. As can be seen, the maximum flow intensity decreases with the magnetic field level up to a critical value, and then increases significantly with the magnetic field level. This critical magnetic field level is somewhere between 2.0 and 3.0 kGauss in this LPEE set up. Below this level the flow is suppressed, but above this level the flow gets stronger. Such behaviour is not surprising, as explained in [16] and also as supported by our experiments [14,15], which

Table 2
Physical properties and growth parameters of the LPEE growth of GaAs

Parameter	Symbol	Value
Growth temperature	T_g	1073 K
Electrical current density	J	3×10^4 to $7 \times 10^4\ \mathrm{A/m^2}$
Peltier coefficient	π_p	0.3 V
Electrical conductivity	σ_E	$2.5 \times 10^6\ \Omega^{-1}\ \mathrm{m}^{-1}$
Thermal conductivity of the solution	k_l	52.6 W/(mK)
Thermal diffusivity	α	$0.3 \times 10^{-4}\ \mathrm{m^2/s}$
Solutal diffusivity	D_C	$4 \times 10^{-9}\ \mathrm{m^2/s}$
Solutal kinematic viscosity	ν	$1.21 \times 10^{-7}\ \mathrm{m^2/s}$
Solution density	ρ_L	$5.63 \times 10^3\ \mathrm{kg/m^3}$
Solutal mobility	μ_E	$0.068 \times 10^{-4}\ \mathrm{m^2/(Vs)}$
Thermal expansion coefficient	β_T	$9.85 \times 10^{-5}\ \mathrm{K}^{-1}$
Solutal expansion coefficient	β_C	0.084
Crystal radius	R_c	0.0120 m
Solution height	H	0.0103 m

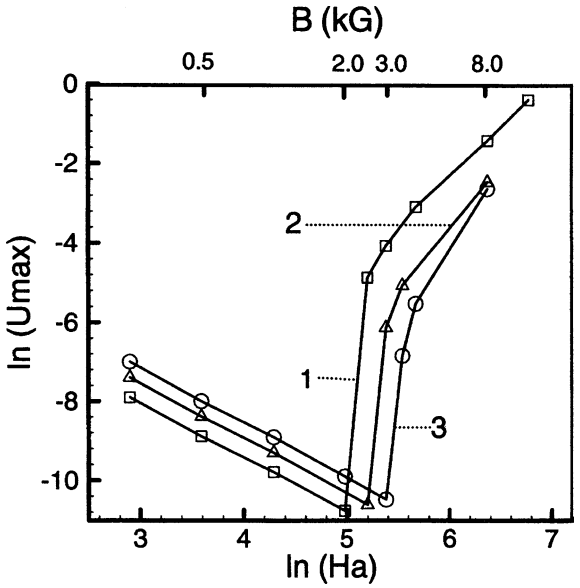

Fig. 2. The computed maximum flow velocity values under various magnetic field levels show a similar pattern under all three electric current densities: (1) $J = 3$ A/cm^2; (2) $J = 5$ A/cm^2; and (3) $J = 7$ A/cm^2. The applied magnetic field suppresses the natural convection in the solution up to a critical value of the applied magnetic field level and then the strength of the flow increases significantly with the magnetic field [24,27,31].

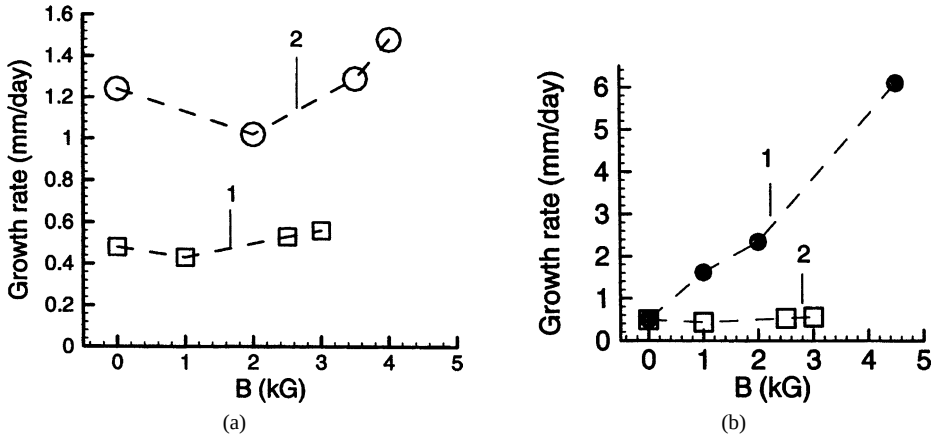

Fig. 3. (a) Computed growth rates are presented versus applied magnetic field with the use of constant electric mobility μ_E. Squares represent the values at $J = 3$ A/cm^2 and circles denote for the values at $J = 7$ A/cm^2. (b) Growth rates computed using the total mobility, $\mu_{\text{total}} = \mu_E + \mu_B$, are presented by full circles. These values are in agreement with the experimental growth rates (hallow circles; but are coincident with the full circles, see Table 1 for their values). The growth rates under no magnetic field are also shown (squares) for comparison [31].

is mainly due to the loss of a delicate balance between the magnetic and gravitational body forces when the field intensity exceeds a certain critical level.

In computations presented in [24,27], only the constant electric mobility μ_E was used. A summary of the growth rates from these numerical simulations is presented in Fig. 3(a). The values under no magnetic field are the experimental growth rates and are used to compute the value of μ_E. Naturally they are coincident with the

computed values. As can be seen, the growth rate decreases first with the magnetic field level and then increases with the magnetic field above the critical value. This pattern is similar to the pattern of experimental growth rates under various magnetic field levels, and also agrees with the numerical simulation results. However, as mentioned earlier and also as presented in [14,15], the experimental growth rates under applied magnetic field are much higher than those of the numerical simulations that are based on our earlier mathematical models. In order to be able to predict such a growth rate, a new electromagnetic mobility $\mu_{\text{total}} = \mu_E + \mu_B$ was used in this work. The numerical values of this mobility were calculated from experiments under various magnetic field levels and presented in Table 1. Growth rates computed using the total mobility μ_{total} are presented in Fig. 3(b) (the full circles), and agree with those of experiments. The growth rates using only the electric mobility μ_E are also given in Fig. 3(b) for comparison (denoted by empty squares). For the sake of completeness and for comparison, the experimental growth rates under magnetic field are also presented in Fig. 3(b) (note that the full and empty circle are coincident).

Fig. 4 summarizes the computed results of [31] for the flow field that are present in the horizontal plane at the middle of the growth cell (left column) and in the vertical plane at $\varphi = 0$ (right column) for three levels of magnetic field strengths ($B = 0.0, 1.0$, and 3.5 kGauss) at $J = 5.0$ A/cm^2. The comparison of flow fields with those of [27] and [24] shows that the inclusion of the interface evolution in computations did not affect the flow fields significantly.

The flow fields under various magnetic field and electric current density levels were computed in [31]. In Fig. 5(a)–(e), the time evolution of the flow under $B = 4.0$ kGauss and $J = 7$ A/cm^2 is shown as an example. As can be seen from these figures the flow patterns change with time, and begin to localize after 240 seconds. The localization is approximately at about a distance of $1/4$ of the diameter of the crystal from the edge. This is where the holes or damages were observed in the experiments of [15] and [16]. It is possible that the strong and localized convection is responsible for unsuccessful experiments at higher fields. The flow pattern at $J = 5$ A/cm^2 and $B = 3.0$ kGauss also show a similar flow pattern after a long period of time (Fig. 5(f)). In terms of flow behaviour, the numerical simulations are in qualitative agreement with experiments, but they do not agree quantitatively

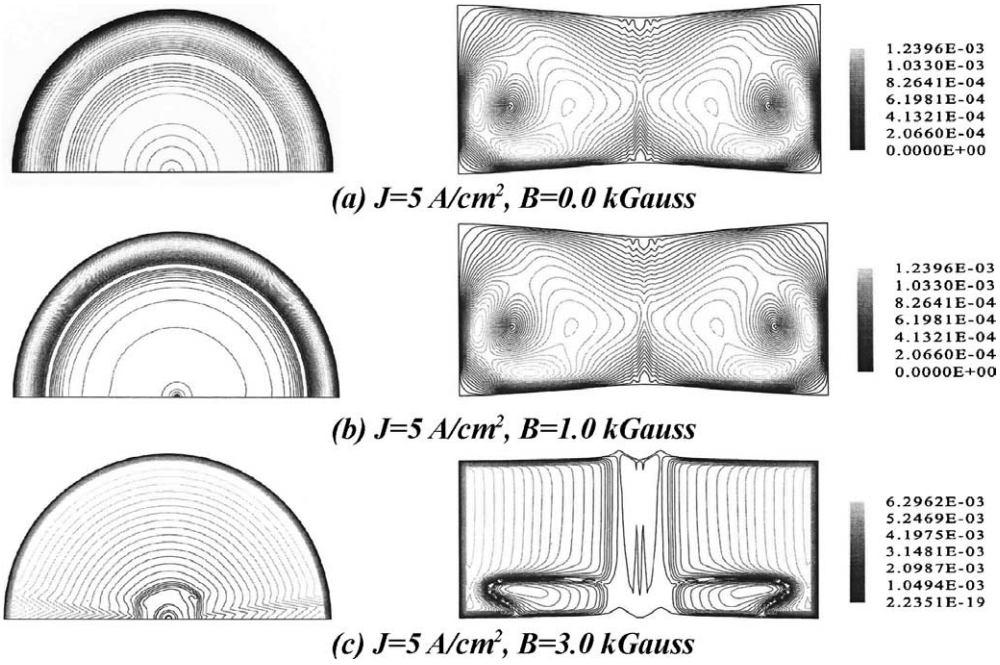

Fig. 4. Flow field (iso-speed contours) under various magnetic field levels. As can be seen from the left in (c), the development of 3-D structures is initiated [27,31].

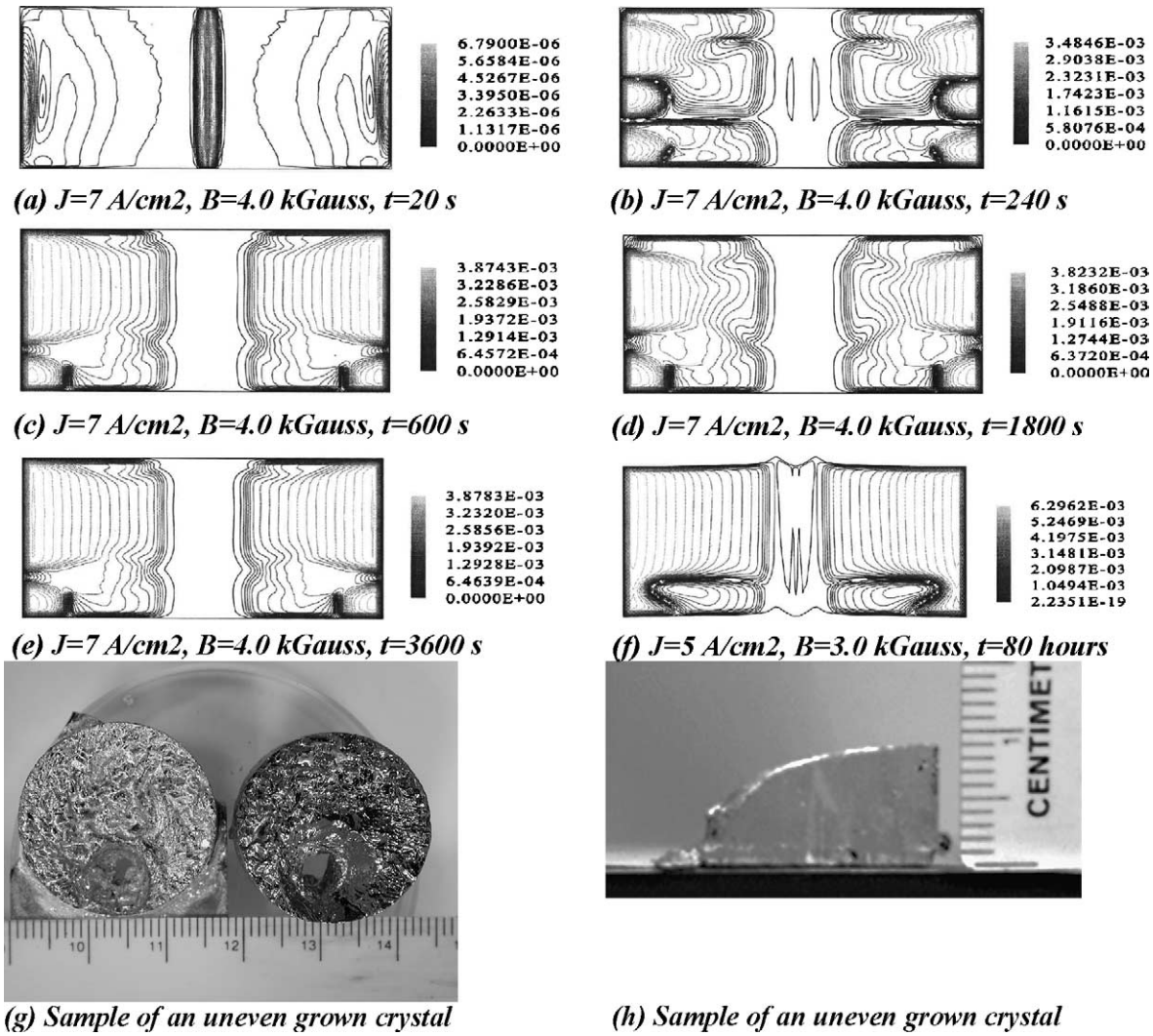

Fig. 5. (a)–(f): Time evolution of the flow field (iso-speed contours). As can be seen from figures (b)–(f), the flow field is very localized near the growth interface at about a distance of 1/4 of the crystal diameter. This location is approximately where the large holes (about 3 mm in diameter) were observed in the grown crystals, as seen in (g). Three of uneven grown crystals are shown: two crystals with hole (top view in (g)), and a half cut of an uneven grown crystal in (h) (in this experiment, the hole was probably so large that destroyed the half the grown crystal) [15,24,27,31].

on the critical value of the magnetic field. Numerical simulations predict a lower value (about 2 kGauss) than the maximum experimental value of 4.5 kGauss. Crystals were successfully grown up to $B = 4.5$ kGauss and $J = 7\ \mathrm{A/cm^2}$ field levels, however, experiments at higher field levels have failed (two samples of such crystals are presented in Fig. 5 (g) and (h) for the sake of comparison [24]. The small qualitative disagreement on the critical magnetic field can be attributed to a number of approximations made in the modelling.

It is important to mention that one may have the impression from Figs. 4 and 5 that the flow structures appears to maintain their initially assumed axisymmetry throughout the simulation. However, although it is not obvious to the naked eye, the flow structures lose their axisymmetry and develop three-dimensional structures in spite of assumed axisymmetric boundary conditions. One can see the development of a three-dimensional structure in the flow field

in Fig. 4(c) on the left. But the effect of three-dimensionality is more prominent in the concentration field. The development of three-dimensional structures in the concentration field can be clearly seen in the numerical results presented in Fig. 6 [24].

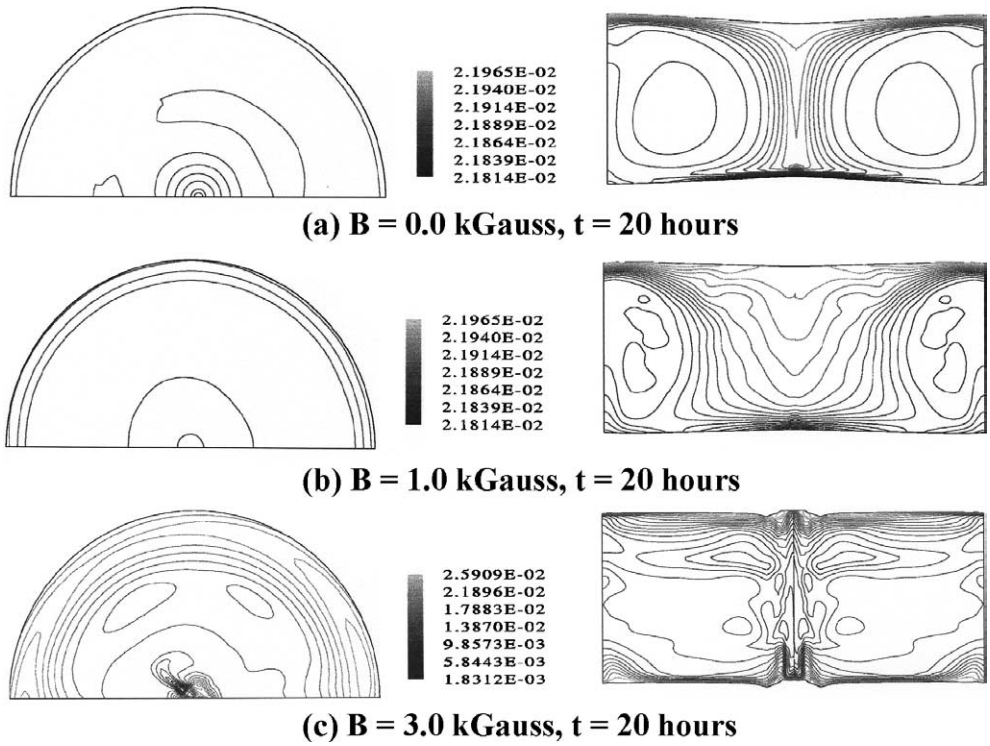

Fig. 6. Concentration distribution at various magnetic field levels. The development of 3-D structures can clearly be seen at high magnetic field level: in (c) at left [24,27].

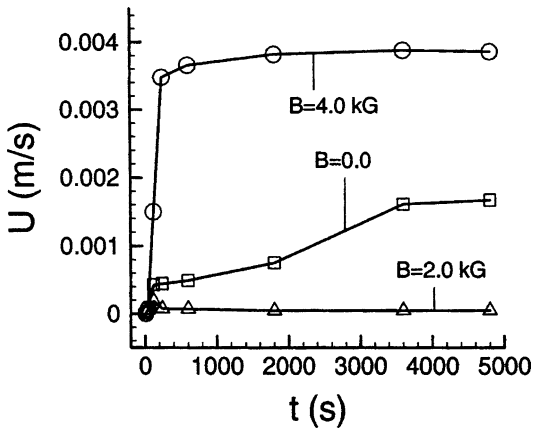

Fig. 7. Transient behaviour of the flow field is presented under three magnetic field levels, $B = 0.0$, 2.0, and 4.0 kGauss. It is obvious that flow is suppressed under low magnetic field levels (less than the critical value). It is also interesting that the flow under magnetic field reaches an almost-steady-state much faster than no magnetic field [31].

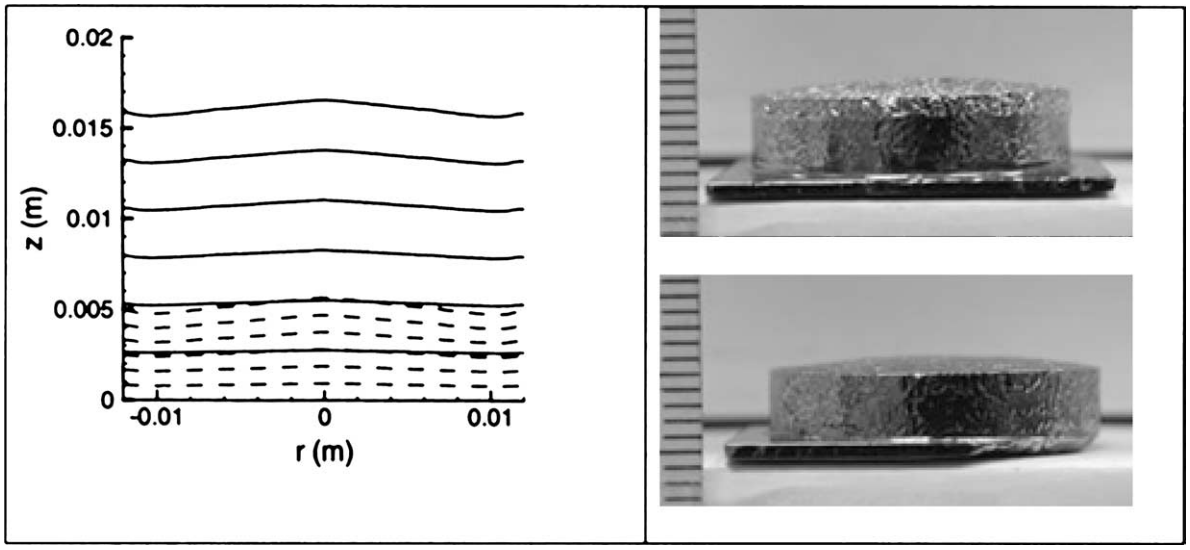

Fig. 8. Evolution of the computed growth interface using the total mobility $\mu_{\text{total}} = \mu_E + \mu_B$. The shapes of the computed interfaces are in excellent agreement with those of experiments [14,15]. This shows that the model introduced in [31] predicts well the experimental interface shapes.

The results for time evolution of the flow intensity are summarized in Fig. 7. As can be seen under the effect of applied magnetic field the fluid flow reaches an almost-steadystate much faster than the case in the absence of a magnetic field.

In Fig. 8 the evolution of growth interface is presented [31]. As can be seen the interfaces are flatter than those obtained through earlier simulations in [27], and they agree with the shapes and interfaces of the crystals grown in [15] and [16] which are almost perfectly flat.

5. Conclusions

Liquid Phase Electroepitaxial (LPEE) crystal growth experiments show that the growth rate under an applied static magnetic field is also proportional with the applied magnetic field, and increases with the increasing field intensity level. Experiments also show that the direction of electromigration of species is in the direction of the applied electric current regardless of whether the applied magnetic field is up or down. The LPEE growth rate under magnetic field is about 12 times higher than that of no magnetic field. Earlier mathematical models developed for the LPEE growth process do not predict this increase in the growth rate. In order to address this important issue a new model for the LPEE growth is introduced, and the increase in the growth rate is incorporated into the mass transport equation. A new electromagnetic mobility, which is linearly dependent on B, is defined in the model to predict the experimental growth rates.

Numerical simulations carried out under various magnetic field and electric current density levels show that the growth rate is proportional with both the electric current density and the magnetic field. The computed flow field in the solution exhibited interesting flow structures. The flow was suppressed up to a critical magnetic field (about 2.0 kGauss), and became very strong at higher magnetic field levels. One can conclude that the application of a static magnetic field is beneficial up to a critical field level, and may be lead to unstable growth at higher fields.

Acknowledgements

The financial support provided by the Microgravity Science Program of the Canadian Space Agency and the Natural Sciences and Engineering Research Council of Canada (NSERC) is gratefully acknowledged.

References

[1] L. Jastrzebski, H.C. Gatos, A.F. Witt, Electromigration in current-controlled LPEE, J. Electrochem. Soc. 123 (1976) 1121.
[2] L. Jastrzebski, Y. Imamura, H.C. Gatos, Thickness uniformity of GaAs layers grown by electroepitaxy, J. Electrochem. Soc. 125 (1978) 1140–1146.
[3] A. Okamoto, L. Lagowski, H.C. Gatos, Enhancement of interface stability in liquid-phase electroepitaxy, J. Appl. Phys. 53 (1982) 1706–1713.
[4] T. Bryskiewicz, C.F. Boucher Jr., J. Lagowski, H.C. Gatos, Bulk GaAS crystal growth by liquid phase electroepitaxy, J. Crystal Growth 82 (1987) 279–288.
[5] T. Bryskiewicz, P. Edelman, Z. Wasilewski, D. Coulas, J. Noad, Properties of very uniform $In_xGa_{1-x}As$ single-crystals grown by liquid-phase electroepitaxy, J. Appl. Phys. 68 (1990) 3018–3020.
[6] T. Bryskiewicz, A. Laferriere, Growth of alloy substrates by liquid phase electroepitaxy – theoretical considerations, J. Crystal Growth 129 (1993) 429–442.
[7] K. Nakajima, Liquid-phase epitaxial-growth of very thick $In_{1-x}Ga_xAs$ layers with uniform composition by source-current-controlled method, J. Appl. Phys. 61 (9) (1987) 4626–4634.
[8] S. Dost, Z. Qin, A model for liquid phase electroepitaxial growth of ternary alloy semiconductors. 1 – Theory, Int. J. Electromagn. Mech. 7 (2) (1996) 109–128.
[9] Z.R. Zytkiewicz, Joule effect as a barrier for unrestricted growth of bulk crystals by liquid phase electroepitaxy, J. Crystal Growth 172 (1997) 259–268.
[10] K. Nakajima, Layer thickness calculation of $In_{1-x}Ga_xAs$ grown by the source-current-controlled method – diffusion and electromigration limited growth, J. Crystal Growth 98 (1989) 329–340.
[11] K. Nakajima, T. Kusunoki, C. Takenaka, Growth of ternary $In_xGa_{1-x}As$ bulk crystals with a uniform composition through supply of GaAs, J. Crystal Growth 113 (1991) 485–490.
[12] Z.R. Zytkiewicz, Influence of convection on the composition profiles of thick GaAlAs layers grown by liquid-phase electroepitaxy, J. Crystal Growth 131 (1993) 426–430.
[13] S. Dost, H. Sheibani, in: Mechanics of Electromagnetic Materials and Structures, in: J.S. Yang, G.A. Maugin (Eds.), Stud. Appl. Electr. Mech., vol. 19, IOS Press, Amsterdam, 2000, pp. 17–29.
[14] H. Sheibani, Liquid phase electroepitaxial bulk growth of binary and ternary alloy semiconductors under external magnetic field, Ph.D. Thesis, University of Victoria, Victoria, BC, Canada, July 2002.
[15] H. Sheibani, S. Dost, S. Sakai, B. Lent, Growth of bulk single crystals under applied magnetic field by liquid phase electroepitaxy, J. Crystal Growth 258 (2003) 283–295.
[16] S. Dost, Z. Qin, A model for liquid phase electroepitaxy under an external magnetic field – 1. Theory, J. Crystal Growth 153 (1995) 123–130.
[17] Z. Qin, S. Dost, N. Djilali, B. Tabarrok, A model for liquid phase electroepitaxy under an external magnetic field. 2. Application, J. Crystal Growth 153 (1995) 131–139.
[18] S. Dost, Recent developments in modeling of liquid phase electroepitaxy: a continuum approach, Appl. Mech. Rev. 49 (12) (1996) 477–495.
[19] Z. Qin, S. Dost, A model for liquid phase electroepitaxial growth of ternary alloy semiconductors. 2. Application, Int. J. Electromagn. Mech. 7 (2) (1996) 129–142.
[20] S. Dost, Z. Qin, A numerical simulation model for liquid phase electroepitaxial growth of GaInAs, J. Crystal Growth 187 (1998) 51–64.
[21] S. Dost, Numerical simulation of liquid phase electroepitaxial growth of GaInAs under magnetic field, ARI – the Bullettin of ITU 51 (1999) 235–246.
[22] S. Dost, Y.C. Liu, B. Lent, A numerical simulation study for the effect of applied magnetic field in liquid phase electroepitaxy, J. Crystal Growth 240 (2002) 39–51.
[23] Y.C. Liu, H. Sheibani, S. Sakai, Y. Okano, S. Dost, in: C.R. Kleijn, S. Kawano (Eds.), Computational Technologies for Fluid/Thermal/Structural/Chemical Systems with Industrial Applications, in: ASME Proc. PVP, vol. 448-1, New York, 2002, pp. 65–72.
[24] H. Sheibani, Y.C. Liu, S. Sakai, B. Lent, S. Dost, The effect of applied magnetic field on the growth mechanisms of liquid phase electroepitaxy, Int. J. Engrg. Sci. 41 (2003) 401–415.
[25] R.W. Series, D.T.J. Hurle, The use of magnetic-fields in semiconductor crystal-growth, J. Crystal Growth 113 (1991) 305–328.

[26] D.T.J. Hurle (Ed.), Handbook of Crystal Growth 2: Bulk Crystal Growth, Part B: Growth Mechanisms and Dynamics, North-Holland, 1994.
[27] Y.C. Liu, Y. Okano, S. Dost, The effect of applied magnetic field on flow structures in liquid phase electroepitaxy – a three-dimensional simulation model, J. Crystal Growth 244 (2002) 12–26.
[28] S. Dost, H.A. Erbay, A continuum model for liquid-phase electroepitaxy, Int. J. Engrg. Sci. 33 (1995) 1385–1402.
[29] A.C. Eringen, G.A. Maugin, Electrodynamics of Continua I and II, Springer, New York, 1989.
[30] Z. Qin, S. Dost, N. Djilali, B. Tabarrok, Finite element model for liquid phase electroepitaxial growth of GaAs crystals, Int. J. Numer. Methods Engrg. 38 (1995) 3949–3968.
[31] Y. Liu, S. Dost, H. Sheibani, A three-dimensional numerical simulation for the transport structures in liquid phase electroepitaxy under applied magnetic field, Int. J. Transport Phenomena, in press.
[32] V. Timchenko, P.Y.P. Chen, G. de Vahl Davis, E. Leonardi, R. Abbaschian, A computational study of transient plane front solidification of alloys in a Bridgman apparatus under microgravity conditions, Int. J. Heat Mass Transfer 43 (2000) 963–980.
[33] V. Timchenko, P.Y.P. Chen, G. de Vahl Davis, E. Leonardi, R. Abbaschian, A computational study of binary alloy solidification in the Mephisto experiment, Int. J. Heat Mass Transfer 23 (2002) 258–268.